On the trigger mechanism of the L-H transition in NSTX

A. Diallo[1], S. Banerjee*, S. Zweben[1], and T. Stoltzfus-Dueck[1]
[1] Princeton Plasma Physics Laboratory, Princeton, NJ, USA.
*Institute for Plasma Research, Bhat, Gandhinagar 382428, Gujarat, India.
E-mail address of main author: adiallo@pppl.gov

Understanding the trigger mechanism that leads to the transition between the low (L) and high (H)-confinement plasma in tokamak devices remains one of the most outstanding theoretical and experimental challenges for fusion science, and it is critical for ITER operation. Motivated by the need to rigorously test the L-H transition models (e.g., predator-prey and ExB flow suppression), while also exploring other possible explanations, we investigate the L-H transition dynamics using tha gas-puff imaging (GPI) of high temporal and spatial resolution on NSTX.

In our analysis using a novel orthogonal decomposition programming (ODP) approach for velocimetry [1], we observe the inferred poloidal velocity to become more positive across the L-H transition (see figure 1) in all types of discharges. Ohmic discharges indicate a decrease of turbulent kinetic energy inside the last-closed flux surface and a reduction in the magnitude of the (negative) production term indicating a decrease of the transfer of energy from the mean flow to the turbulence. In RF- and NBI-heated discharges, however, the kinetic energy in the turbulence continues to increase across the L-H transition. Such increase is consistent with a negative production term. These observations are at odds with the predator-prey model often proposed as a mechanism for the L-H transition.

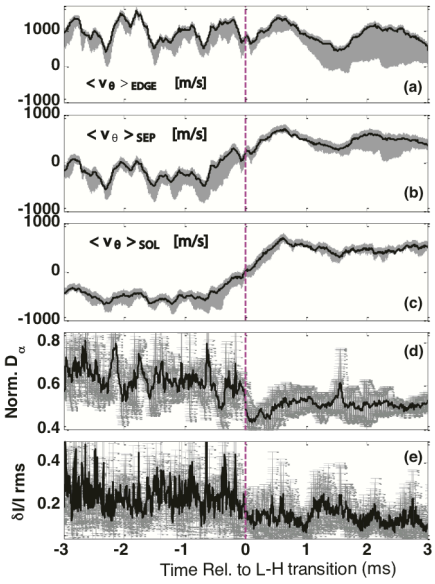

Figure 1: (a) –(c) Time evolution of the inferred poloidal velocity, poloidally averaged for multiple Ohmic discharges for three radial positions; (a) inside the LCFS, (b) at the separatrix and (c) in the SOL. (d) The drop in the averaged normalized Dalpha for all the discharges indicated the L-H transition. (e) GPI intensity rms fluctuations.

Here, we report on the investigation of the L-H trigger mechanism for three sets of discharges (ohmic, RF, and NBI) using an edge localized turbulence imaging system, namely GPI. This system has a temporal resolution of 2.5 μs per frame and up to ~ 1 cm spatial resolution over 24 x 30 cm at the outer midplane edge of NSTX. Based on the GPI enhanced temporal and spatial resolution, a velocimetry analysis using the novel orthogonal ODP approach provides the edge 2D velocity field at very high spatial and temporal resolution across the L-H transition.

Motivated by Cziegler's [2] results that suggested a time sequence for the L-H transition, namely, the peaking of the Reynolds power and then a collapse of the turbulence and finally the rise of the diamagnetic electric field, we are testing this timeline on the L-H transition data base in NSTX in order to study the trigger mechanism, with careful accounting for experimental uncertainties.

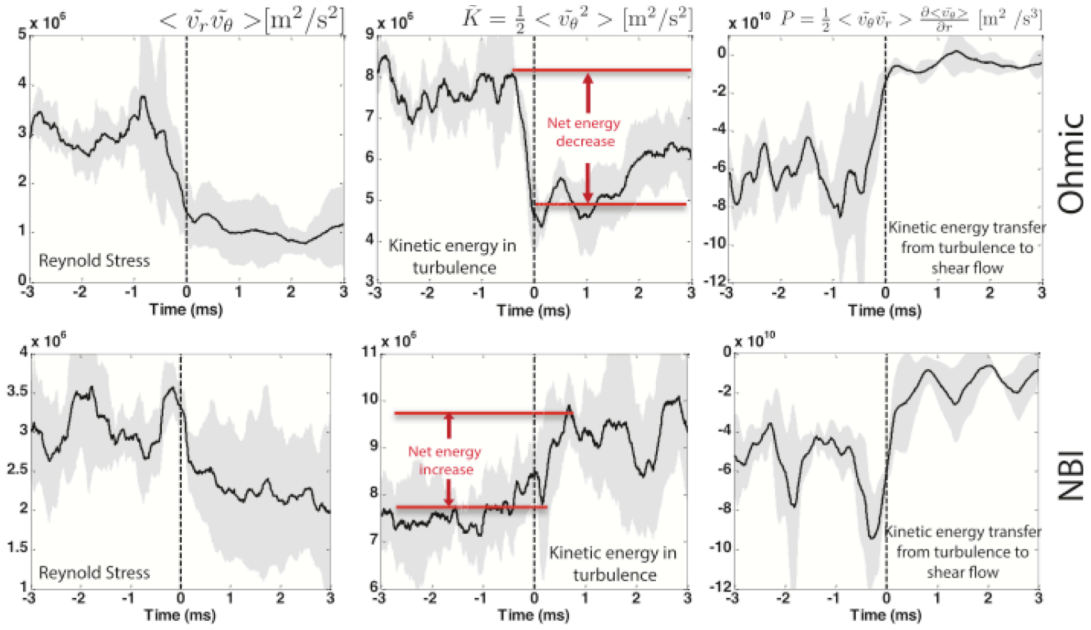

Figure 2: Time evolution of the Reynolds stress, the kinetic energy of the turbulence and its transfer to shear flow at 1 cm inside the separatrix. The **top row** respresents Ohmic discharges parameters and the **bottom row** the NBI discharges. The grey represents the root-mean-square deviations over multiples dicharges.

To diagnose this triggering mechanism given the nonstationarity of the signals, the velocity field dynamics is studied using the ODP in the framework of the k-e model [4]. The model equations underlying the data analysis are given as follows: $\partial_t \tilde{K} = \gamma_{eff}\, \tilde{K} - P - \partial_r \tilde{T}$ and $\partial_t \bar{K} = P - \partial_r \bar{T} - \nu_{LF} \bar{K}$. P represents the production term (energy transfer from turbulence to zonal flows) and is defined as $\langle \tilde{v}_\theta \tilde{v}_r \rangle \partial_r \langle \bar{v}_\theta \rangle$. $\tilde{K}$ and $\bar{K}$ represent the turbulence and mean kinetic energy, respectively. We define $\bar{T} = \langle \tilde{v}_\theta \tilde{v}_r \rangle \langle \bar{v}_\theta \rangle$ and $\tilde{T} = 0.5 \langle {\tilde{v}_\theta}^2 \tilde{v}_r \rangle$. Finally, γ_{eff} and ν_{LF} account for the net effective linear growth and the damping rate of the high and low frequency components, respectively (see refs Cziegler [2] and Manz [3] for a detailed description of these equations). Note that the fluctuating components of the velocities are represented by frequencies greater than 5 kHz and the mean components by frequencies below 3 kHz.

Figure 2 displays an example of the temporal evolution across the L-H transition of the Reynolds' stress, the turbulent kinetic energy, and the production term during an Ohmic discharge. The L-H transition appears to be preceeded (within 350 – 400 μs) by a decrease of the Reynolds stress and the turbulence kinetic energy. (Note that the temporal resolution is 250 μs). These decreases are accompanied with a negative production term, which suggests a transfer from DC flows to turbulence. This is at odds with the general predator-prey picture. In NBI and RF-heated plasmas the fluctuation kinetic energy increases across the L-H transition, while the Reynolds' stress decreases. Again, a negative production term is observed. Overall, these results are different than the time sequence of the L-H transistion and the positive production term (transfer from turbulence to DC flows) increasing before the L-H transistion as highlighted by Cziegler. In summary, L-H transition studies using GPI data from 17 discharges in NSTX appears to be at odds for the ohmic, NBI, and RF cases with L-H transition time sequence put forward by C-Mod results and the ExB L-H transition models. Additional studies of the radial correlation dynamics across the L-H transition will be reported. This work was perfomed under US DoE contract # DE-AC02-09CH11466 at PPPL.
[1] Banerjee et. al., Rev. Sci. Instrum. 86, 033505 (2015); [2] Cziegler et al., Plasma Phys. Control. Fusion 56 075013 (2014); [3] Manz et al., Phys. Plasmas 19 072311 (2012); [4] Tennekes and Lumley, First Course in Turbulence, MIT press. Chap 3.